MICROSTRUCTURE AND MECHANICAL PROPERTIES COMPARISON OF 316L PARTS PRODUCED BY DIFFERENT ADDITIVE MANUFACTURING PROCESSES

Mihaela Nastac, Rick Lucas Andrew Klein

ExOne, Irwin, PA

Abstract

316L stainless steel alloy is well known for its corrosion resistance and combination of strength and ductility. By using direct metal additive manufacturing, 316L parts can be produced with volumes and complexity that were previously unachievable. Three of the major metal additive manufacturing technologies – binder jetting, electron beam melting, and selective laser melting – produce SS316L parts, but with different material properties and microstructures. This paper will examine the microstructure and mechanical properties differences between parts produced by the three methods and discuss recent advances to improve microstructure and mechanical performance of metallic alloy parts produced by additive manufacturing.

Introduction

A detailed comparison of three different additive manufacturing (AM) technologies in terms of microstructure and mechanical properties of a 316L stainless steel alloy is presented in this study. The selected AM technologies are: (1) Binder Jetting Additive Manufacturing (BJ), (2) Electron Beam Melting (or EBM) and (3) Direct Metal Laser Sintering (DMLS). These main technologies are widely used to fabricate parts for various commercial applications related to energy, automobile, and aerospace industries. The BJ technology, which was developed by Exone, was employed to produce the samples, which were then evaluated for microstructure and mechanical properties in this study. The EBM Samples were supplied by Oak Ridge NL, while the DMLS samples were produced by Proto labs.

Experimental Procedure for BJ Process

Both the EBM and the DMLS technologies are presented in the literature [1-3]. BJ technology is described in the following paragraphs.

BJ technology is an additive manufacturing process capable of printing relatively large parts. The process consists of selectively depositing a liquid binder to join powder particles forming a voxel as shown in Fig. 1a. Figure 1b illustrates the deposition of the liquid binder during the printing process.
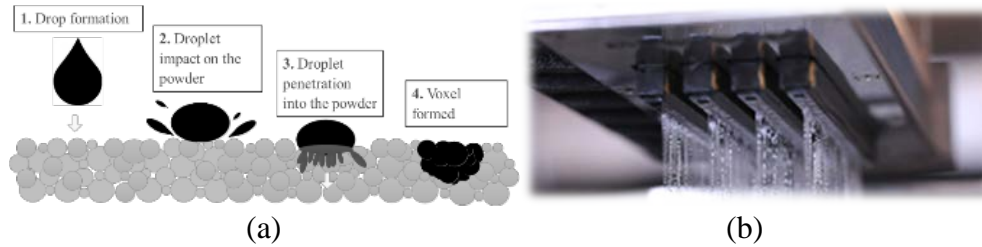
Figure 1. The formation of voxels in the BJ process (a) and the printer head dispending the liquid binder during the printing process (b).

As the print-head passes over a layer of powder, binder is deposited onto the powder. The job-box lowers and a subsequent layer of powder is spread; the print-head passes again, depositing binder onto the second layer of powder. The part develops through the layering of powder and binder, until a near-net shape object is achieved.

While other additive manufacturing techniques, produce parts with thermally-induced residual stresses and distortions due to large thermal gradients, BJ does not employ heat during the build process, therefore the parts are virtually stress free at the end of the printed cycle. During the printing process, the parts are supported by the loose powder in the job box, therefore eliminating the need for a build plate. After the part is printed, it undergoes a curing and sintering cycle to become the finished part. The samples used in this study were created using this approach. An Innovent ExOne powder bed binder jet printer was used to produce 316L stainless steel samples with the following printing parameters: layer height of 50 μm, recoat speed of 150 mm/s, oscillator speed of 2200 rpm, roller rotation speed of 250 rpm, roller traverse speed of 8 mm/s, and drying speed of 7 mm/s. The 316L powder chemical composition provided by the manufacturer is given in Table 1. The water based binder used in this study is made of ethylene glycol monobutyl ether (CAS # 111-76-2) and ethylene glycol (CAS #107-21-1) [4].

Table 1. Chemical composition of 316L alloy

Element	Cr	Ni	Mo	Mn	Si	P	C	S	Fe
Chemical composition [wt. %]	16.0-18.0	10.0-14.0	2.0-3.0	Max 2	Max 1	Max 0.04	Max 0.03	Max 0.03	balance

In order to perform a microstructural analysis of the processed samples, sections were cut from the specimens, mounted, ground and polished. After surface preparations, the samples were etched with a Glyceregia solution and then optical microscopy (OM) micrographs were taken. Microstructural characterizations and compositional analyses were also conducted using Scanning Electron Microscopy (SEM) equipped with Energy Dispersive X-ray Spectroscopy.

Experimental Results and Discussion

Microstructure characterizations of the 316L stainless steel sample produced via BJ process were performed on the etched surface using OM and SEM. The chemical composition of the precipitates was determined by an Energy Dispersive X-Ray Spectroscopy (EDS) detector (OmegaMax Express SEM/EDS). The OM micrographs, taken on the polished surface (Figure 2

(a) and (b)), reveal a largely compact material with few fine pores, which are randomly distributed. The microstructure of the etched sample is shown in Fig. 3 (a), (b) and (c). The specimen consists of an equiaxed grain structure, with a grain size ranging from 30µm to 60µm. The precipitates are primarily observed at the grain boundaries. Few precipitates are also found inside the grains. The EDS elemental analysis for different areas of the sample are consistent with the SS316L austenite matrix as well as with some precipitates with a higher amount of Carbon and Oxygen, as it can be observed from Fig. 5 (b) and Table 2, location #7.
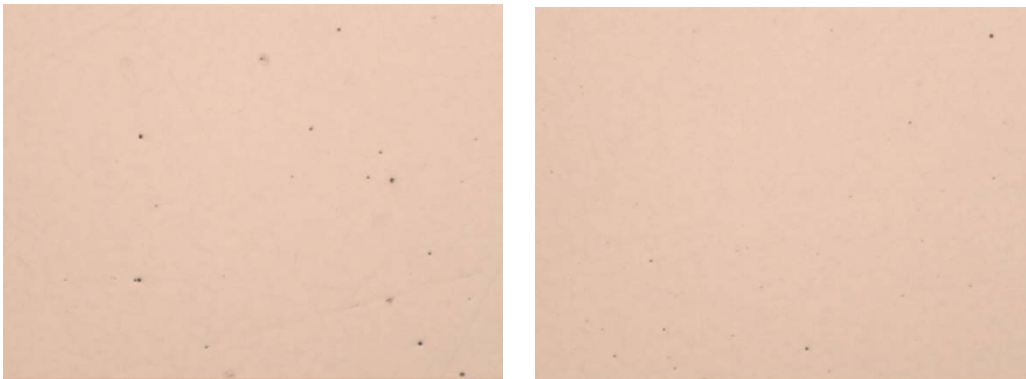

Figure 2. OM micrographs (50x) of the 316L polished sample showing porosity distribution.
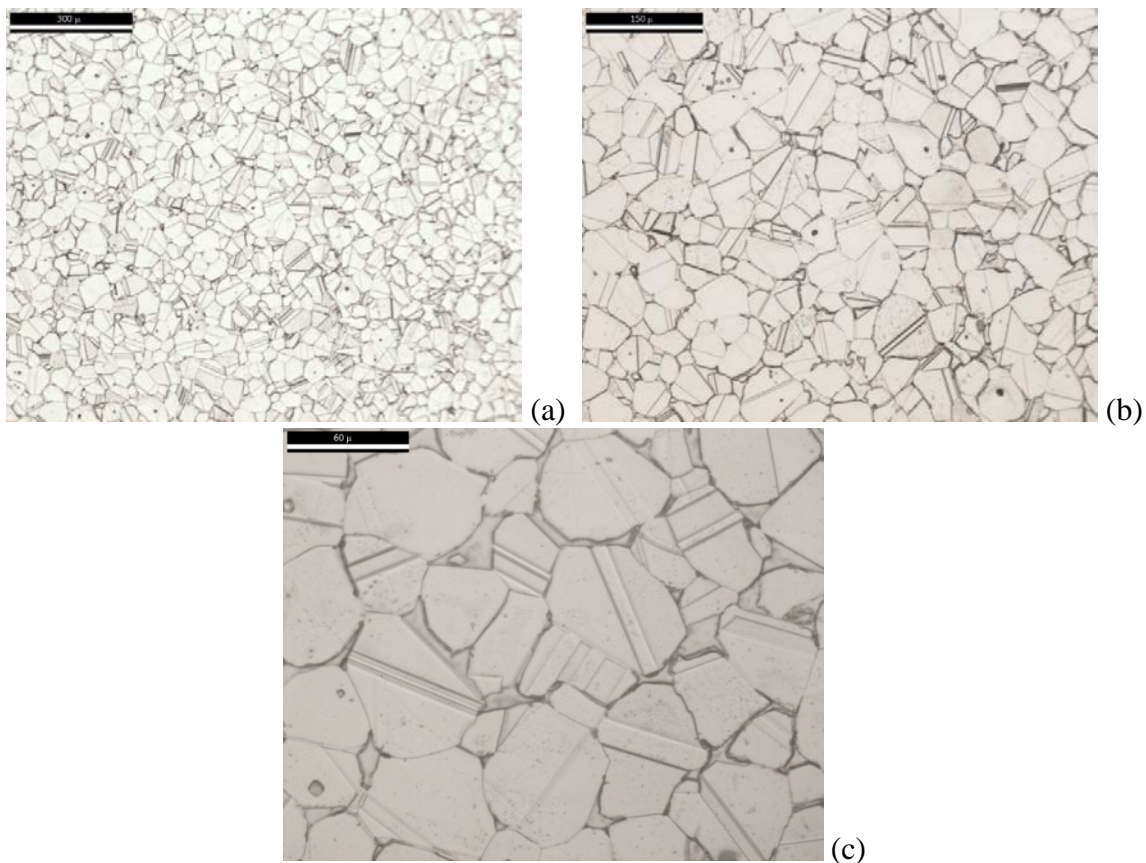

(a)

(b)

(c)

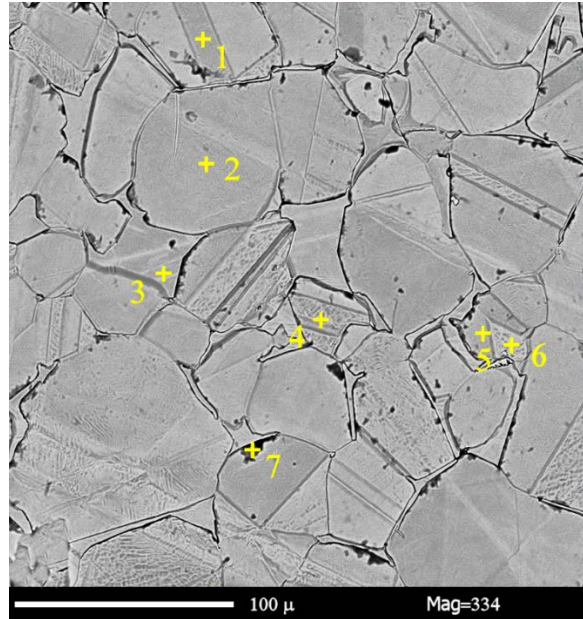Figure 3. OM micrographs of the 316L sample in as etched condition (Glyceregia etchant): a) 100x; b) 200x; c) 500x.

Figure 4. SEM image of the 316L BJ etched sample.

(a): EDS elemental analysis 1
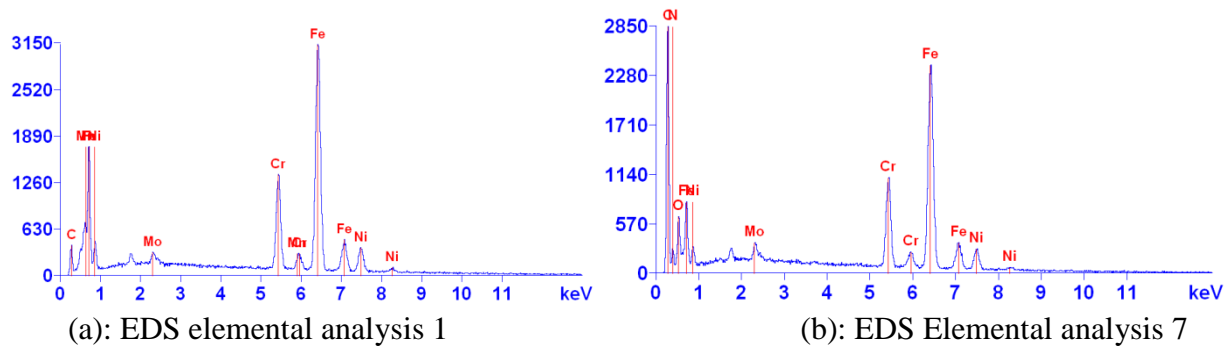
(b): EDS Elemental analysis 7

Figure 5. 316L BJ; EDS elemental spectrum analysis (a) location 1 (b) location 7.

Table 2. Compositional analysis (in wt. %) of the 7 points selected on the 316L BJ sample, as shown in Fig. 4

	#1	#2	#3	#4	#5	#6	#7
B	0.0	0.0	0.0	0.0	0.0	0.0	0.0
C	3.9	4.4	4.2	4.7	4.6	4.9	24.5
N	0.0	0.0	0.0	0.0	0.0	0.0	1.2
O	0.0	0.0	0.0	0.0	0.0	0.0	10.1
Si	0.4	0.4	0.4	0.4	0.4	0.4	0.3
P	0.0	0.1	0.1	0.0	0.0	0.1	0.0
S	0.0	0.2	0.2	0.1	0.0	0.1	0.3
Cr	18.4	18.8	25.5	18.4	19.1	19.1	13.1
Mn	1.7	1.1	1.1	1.4	1.6	1.3	0.7
Fe	63.9	63.5	61.1	64.3	63.0	63.7	42.1
Ni	10.5	10.5	4.5	9.6	9.5	9.0	6.7
Mo	1.2	1.1	2.9	1.1	1.7	1.4	1.0

Typical mechanical properties of the as sintered 316L BJ components are shown in Table 3. The values meet and exceed the requirements included in the B-883-15, Standard Specification for Metal Injection Molded Materials: MIM-316L (as sintered) [5].

Table 3. Typical mechanical properties for 316L B

Material	Ultimate strength, MPa	Yield Strength, MPa	Elongation at Break, %	Hardness, HRB	Density, g/cm³
316L	517	214	43	66	7.7

Comparison of microstructure and mechanical properties of BJ, EBM, and DMLS Samples

The mechanical properties of the processed samples are influenced by the size, shape and distribution of the pores, as well as by the size and shape of the grains. Typical values for the mechanical properties of the 316L alloy produced by the BJ, EBM, and DMLS processes, as well as the B883 Standard Specification for Metal Injection Molded Materials, are shown in Table 4.

Table 4: 316L mechanical properties [1, 5, 6].

Additive Manufacturing Process	Ultimate strength, MPa	Yield Strength, MPa	Elongation at Break, %	Hardness, HRB	Density, g/cm³
BJ	517	214	43	66	7.7
EBM [1]	509 ± 3	253 ± 3	59 ± 3		
DMLS [5]	482	172	30	77	
MIM [6]	450	140	40	67	7.6

The optical micrographs of the EBM 316L stainless steel sample are shown in Figure 6 (a) and (b). The mounted specimen was polished and then etched. The as polished surface reveals a largely compact material with few relative large pores as well as fine pores, randomly distributed.

The microstructure of the etched sample shown in Fig. 7 (a) and (b) reveals tiered microstructures, including columnar grain structure, with a grain size in the range of 300-400µm. Fig. 8 shows the point locations of the EDS elemental analysis and Fig. 9 (a); (b), the EDS elemental analysis spectrum for locations #4 and #7.

The complete compositional analysis (in wt. %) of the points are shown in Table 5. The chemical composition of the points indicates consistency with the SS316L matrix, as well as some Carbon and Oxygen rich areas (Table 5, reading #6 and #7).
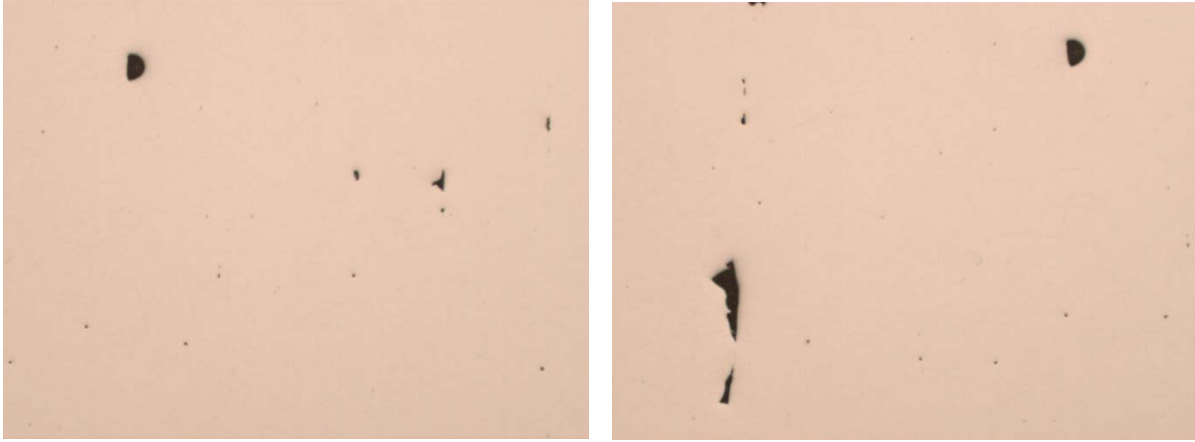
Figure 6. OM micrographs (50x) of the 316L EBM sample in as polished condition.
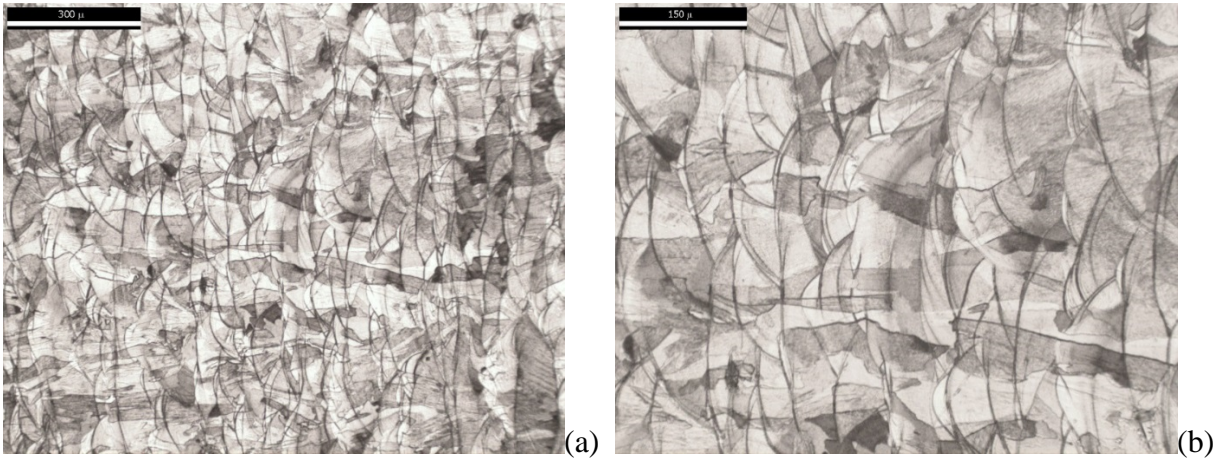

(a)

(b)

Figure 7. OM micrographs of the 316L EBM sample etched with the Glyceregia etchant: (a) 100x; (b) 200x.

Figure 8. SEM image of the 316L EBM etched sample.

(a): EDS elemental analysis 4   (b): EDS elemental analysis 7
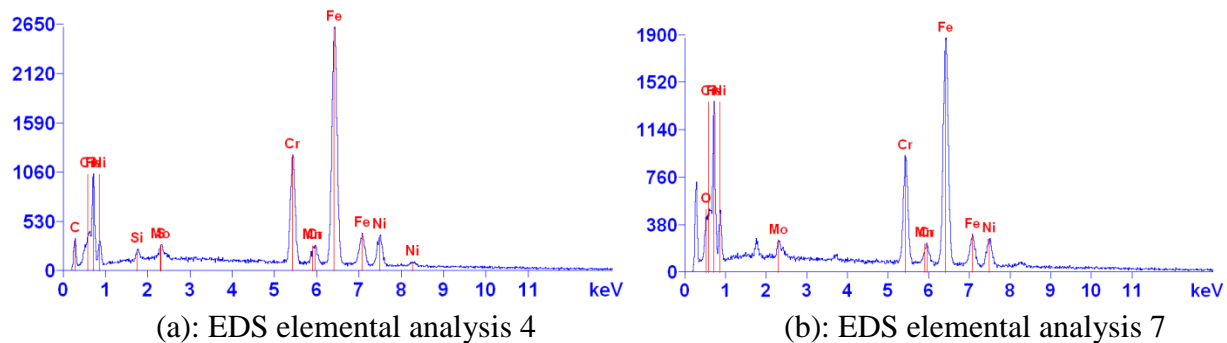
Figure 9: 316L EBM sample: EDS elemental spectrum analysis: (a) location 4 (b) location 7.

Table 5. Compositional analysis (in wt. %), for the 7 points selected on the EBM 316L sample, as shown in Fig. 8.

	#1	#2	#3	#4	#5	#6	#7
B	0.0	0.0	0.0	0.0	0.0	0.0	0.0
C	3.9	3.6	4.1	4.0	5.6	14.0	10.4
N	0.0	0.0	0.0	0.0	0.0	0.0	0.0
O	0.5	0.0	0.0	0.0	0.6	13.0	3.4
Si	0.5	0.4	0.4	0.3	0.4	0.4	0.5
P	0.0	0.0	0.0	0.0	0.1	0.1	0.1
S	0.1	0.0	0.2	0.2	0.0	0.0	0.0
Cr	19.4	19.5	19.8	19.8	19.1	14.7	18.0
Mn	1.6	1.4	1.1	1.3	2.4	1.3	1.4
Fe	61.2	60.8	61.7	61.6	58.5	45.7	54.2
Ni	11.7	12.2	11.5	11.8	11.7	8.7	9.5
Mo	1.2	2.0	1.3	1.0	1.6	2.1	2.6

The OM micrographs of the DMLS 316L are shown in Fig. 10 (a) and (b) in as polished condition, and in Fig. 11 (a) and (b) in as etched condition. Generally, the OM micrographs show a similar tiered microstructure as the EBM sample, with a similar columnar grain structure. The grain size is in the range of 80µm to 150µm. A few larger pores as well as fine pores exist inside the specimen.

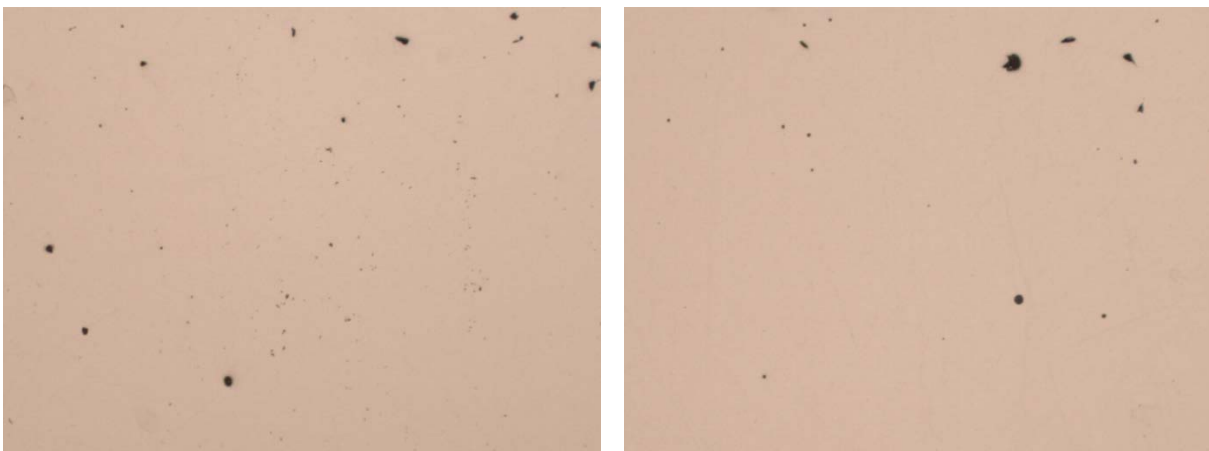Figure 10. OM micrographs (50x) of 316L DMLS sample in "as polished" condition.

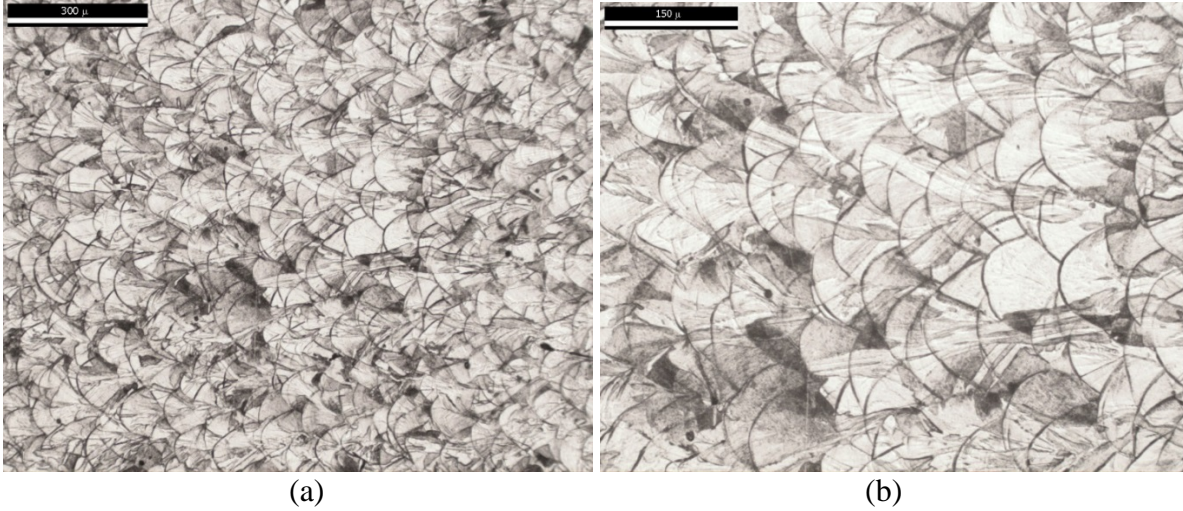(a)   (b)

Figure 11. 316L DMLS sample in as etched condition (Glyceregia etchant); optical microscopy,
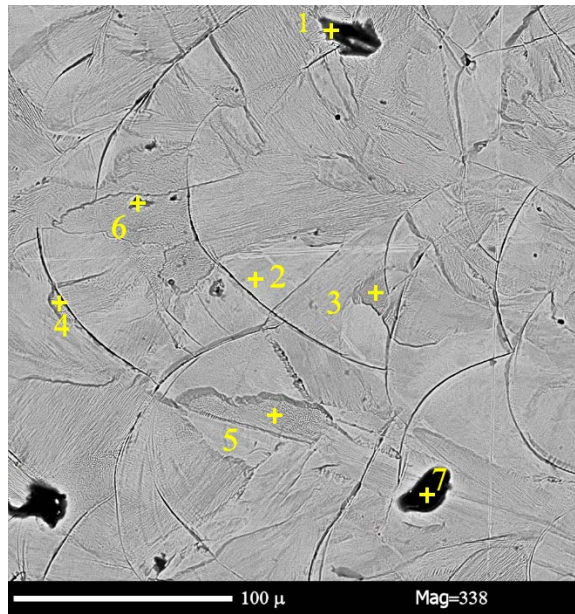(a) 100x; (b) 200x.

Figure 12. SEM image of the 316L DMLS etched sample.

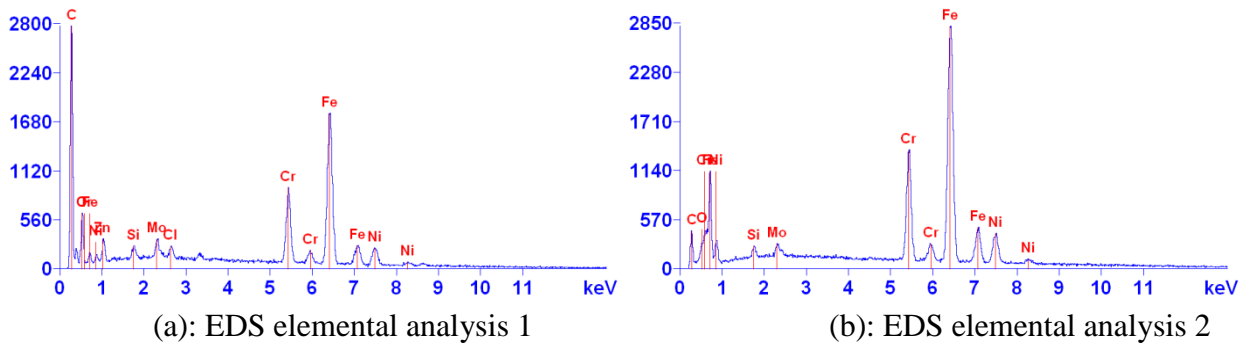(a): EDS elemental analysis 1   (b): EDS elemental analysis 2

Figure 13: 316L DMLS sample: EDS elemental spectrum analysis: (a) location 1 (b) location 2

Fig. 12 shows the point locations of the EDS elemental analysis and Fig. 13 (a) and (b), the EDS elemental analysis spectrum for locations #1 and #2. The complete compositional analysis (in wt. %) of the points are shown in Table 6.

Table 6. Compositional analysis (in wt. %), of the 7 points selected on the 316L DMLS sample, as shown in Fig. 12

	#1	#2	#3	#4	#5	#6	#7
B	0.0	0.0	0.0	0.0	0.0	0.0	0.0
C	28.5	4.5	4.8	4.9	4.7	18.9	70.9
N	0.0	0.0	0.0	0.0	0.0	0.0	0.0
O	12.9	0.0	0.2	0.0	0.0	9.6	19.3
Si	0.4	0.4	0.4	0.4	0.4	0.4	0.4
P	0.0	0.0	0.0	0.1	0.1	0.1	0.2
S	0.2	0.0	0.2	0.0	0.0	0.0	1.4
Cr	12.2	19.6	18.6	19.4	18.6	14.3	1.5
Mn	0.7	1.0	1.5	1.3	1.1	0.6	0.0
Fe	37.5	61.7	62.0	61.0	61.9	46.9	5.1
Ni	6.1	11.3	11.3	11.4	11.9	8.0	0.5
Mo	1.5	1.5	1.1	1.5	1.4	1.2	0.7

Conclusions

Microstructure characterization and analysis of the 316L stainless steel alloy produced by 3 different AM processes was performed in this study. The data showed that while the EBM and DMLS processes are conducive to comparable columnar grain microstructures, the BJ process is generating a relatively fine equiaxed grain microstructure, as illustrated in Fig. 14.

The size and the shape of the grains are essential factors in defining the mechanical properties of the components. An equiaxed grain structure is known to produce isotropic properties and therefore, regardless of the built direction, the components are displaying similar mechanical properties in X, Y and Z directions. Another advantage of the BJ process as related to the 316L alloy is the lack of chemical segregation at the grain boundary, since the process does not involve melting and solidification. This is another key factor that together with an isotropic microstructure will lead to uniform and improved mechanical properties of the final BJ product.
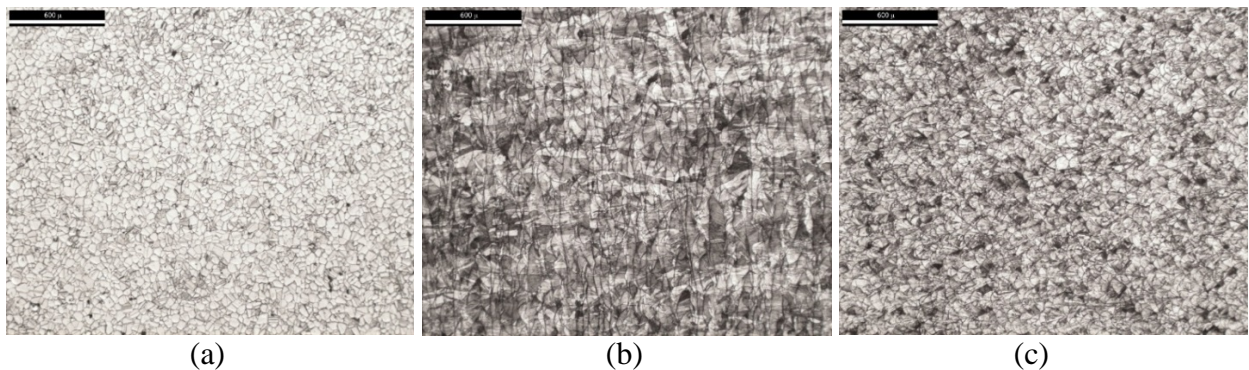

(a)   (b)   (c)

Figure 14. OM micrographs of the 316L samples in etched condition (Glyceregia etchant): (a) BJ 50x; (b) EBM 50x; (c) DMLS 50x;

Acknowledgement

References

[1] Y. Zhong, L.E. Rannar , L. Liu , A. Koptyug , S. Wikman , J. Olsen, D. Cui, Z. Shen, Additive manufacturing of 316L stainless steel by electron beam melting for nuclear fusion applications, *Journal of Nuclear Materials*, vol. 486, 2017, pp. 234-245.

[2] E. Fitzgerald, W. Everhart, The Effect of Location on the Structure and Mechanical Properties of Selective Laser Melted 316L Stainless Steel;, Solid Freeform Fabrication 2016: *Proceedings of the 26th Annual International Solid Freeform Fabrication Symposium – An Additive Manufacturing Conference*, 2016, pp. 1-10.

[3] L.E. Murr, E. Martinez, S.M. Gaytan, D.A. Ramirez, B.I. Machado, P.W. Shindo, J.L. Martinez, F. Medina, J. Wooten, D. Ciscel, U. Ackelid, and R.B. Wicker, Microstructural Architecture, Microstructures and Mechanical Properties for a Nickel-Base Superalloy Fabricated by Electron Beam Melting, *Metallurgical and Materials Transactions A*, vol. 42A, 2011, pp. 3491-3508, DOI: 10.1007/s11661-011-0748-2.

[4] A. Mostafaei, E. L. Stevens, E. T. Hughes, S. D. Biery, C. Hilla, M. Chmielus, Powder bed binder jet printed alloy 625: Densification, microstructure and mechanical properties, *Materials and Design*, vol. 108, 2016, pp. 126–135.

[5] Direct Metal laser Sintering Stainless Steel 315L, Product Specification, ProtoLabs, website: https://www.stratasysdirect.com/wp-content/themes/stratasysdirect/files/material-datasheets/direct_metal_laser_sintering/dmls-stainless-steel-316L-material-specifications.pdf

[6] ASTM B883 Standard Specification for Metal Injection Molded Materials: https://www.astm.org/Standards/B883.htm